

Synergetic Effect of Aluminum and Fluorine Simultaneously Doped Zinc Oxide Thin Films Deposited by Simplified Spray Pyrolysis Technique

H. SONIA JUDITH^a, R. ASHOK KUMAR^{a,*},
A. PANNEERSELVAM^b AND K. SARAVANAKUMAR^c

^a*PG and Research Department of Physics, Thiruvalluvar Government Arts College, Rasipuram, Namakkal, 637 401 Tamil Nadu, India*

^b*Department of Physics, Vivekanandha College of Engineering for Women (Autonomous), Elayampalayam, Tiruchengode, Namakkal, 637 205 Tamil Nadu, India*

^c*Department of Physics, Mahendra Institute of Technology (Autonomous), Mallasamudram, Namakkal, 637 503 Tamil Nadu, India*

Received: 13.08.2024 & Accepted: 19.12.2024

Doi: [10.12693/APhysPolA.147.55](https://doi.org/10.12693/APhysPolA.147.55)

*e-mail: rajamaniashokkumar@gmail.com

The aim of the present investigation is to fabricate pure and aluminum (Al) + fluorine (F) simultaneously doped zinc oxide films using a cost-effective simplified spray pyrolysis technique with a perfume atomizer for the first time. The results report the effects of [Al + F] doping on the structural, optical, electrical, and surface morphological properties of ZnO thin films. The crystalline structure studies reveal the hexagonal wurtzite structure of the ZnO thin films. X-ray diffraction patterns show that the crystallite size decreases from 71.20 to 41.36 nm. Optical studies reveal an average transmittance of 90 at.% in the visible region. The blue shift is observed in the absorption edge, and the band gap value significantly varies from $E_g = 3.25$ eV to $E_g = 3.38$ eV. Electrical studies indicate that the minimum sheet resistance of $58.75 \Omega^{-1}$ is achieved for 3 + 10 at.% of [Al + F] doping. The highest figure of merit is estimated to be approximately $8.441 \times 10^{-3} \Omega^{-1}$. Scanning electron microscope results show a spherical-shaped, pinhole morphology. These findings suggest that the described conditions are very suitable for optoelectronic applications.

topics: zinc oxide, optical, electrical, thin films

1. Introduction

In the past few decades, the dimensionality of materials (1D, 2D, and 3D) has played a vital role in device fabrication. Among these, 2D materials have gained prominence in the fabrication of various technologies, including solar cells, sensors, transistors, computer devices, and LEDs. In particular, transparent conducting metal oxides (TCMOs) such as CdO, TiO₂, In₂O₃, SnO₂, and ZnO have been widely proposed as window layers in numerous studies [1–5]. Among TCMOs, zinc oxide (ZnO) stands out as a versatile material due to its wide band gap ($E_g = 3.37$ eV), high exciton binding energy (60 meV), natural abundance, and chemical stability [6]. Moreover, ZnO is a cost-effective and environmentally friendly material. Its wide band gap makes it suitable for a variety of applications,

including optoelectronic devices, photocatalysis, and biological systems. However, the stoichiometric nature of ZnO results in high electrical resistivity, which limits its performance in some applications. To address this, doping with various elements — such as Al, In, Sn, N, and F — has been extensively explored [7–11]. A promising solution to enhance ZnO's electrical conductivity involves introducing cationic and anionic dopants into its crystal matrix. Recent studies have shown that Al-doped ZnO significantly improves electrical conductivity without compromising optical transmittance, making it a viable alternative to expensive indium tin oxide (ITO) films. Additionally, fluorine doping not only enhances electrical conductivity but also serves as a cost-effective anion substitute for indium. Simultaneous doping with Al³⁺ and F⁻ is particularly interesting because it leverages the dual doping effects: cationic Al³⁺ substitutes for Zn²⁺, while anionic

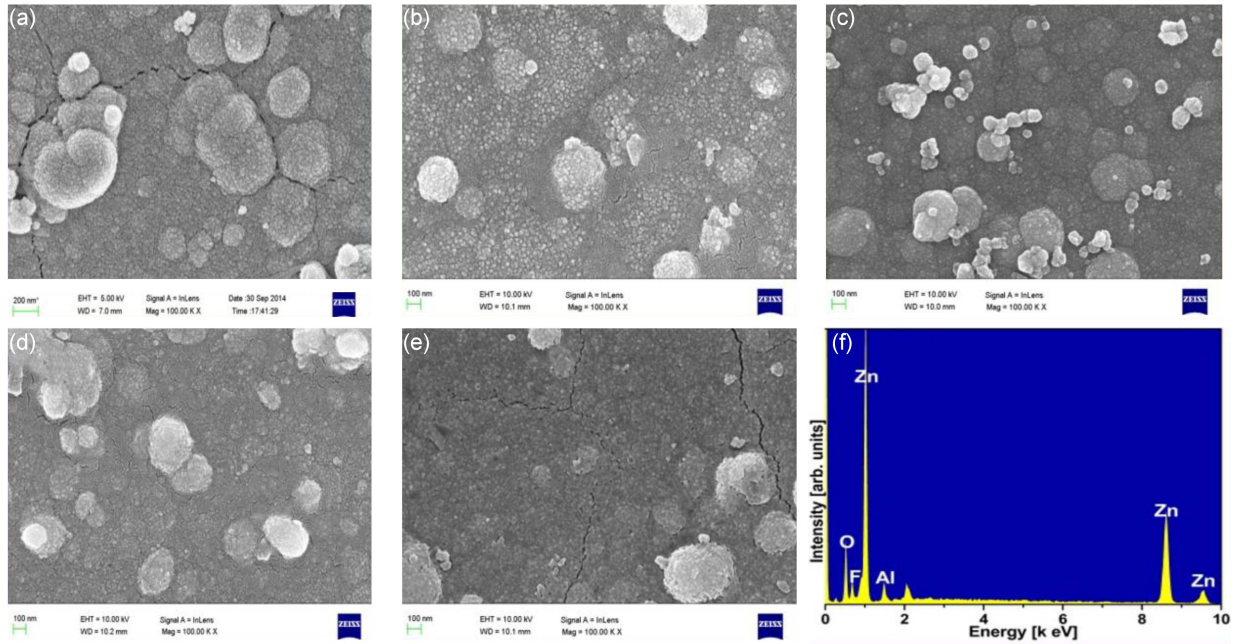


Fig. 1. SEM images of different [Al + F]-doped ZnO films: (a) 0 + 0 at.%, (b) 3 + 5 at.%, (c) 3 + 10 at.%, (d) 3 + 15 at.%, (e) 3 + 20 at.%, (f) EDAX spectrum (3 + 20 at.%).

F^- replaces O^{2-} in the ZnO crystal lattice. ZnO thin films have been deposited using various methods, including sputtering [12], chemical vapor deposition [13], chemical bath deposition [14], successive ionic layer adsorption and reaction (SILAR) [15], sol-gel [16], and spray pyrolysis [17]. Among these, simplified spray pyrolysis stands out due to its simplicity, cost-effectiveness, ease of doping, and ability to coat large areas efficiently.

In the present study, ZnO thin films simultaneously doped with Al and F were fabricated using a simplified spray pyrolysis technique for the first time. The obtained thin films were systematically characterized for their structural, optical, electrical, and surface properties, and the results are reported in detail.

2. Materials and method

2.1. Preparation of pure ZnO and $Zn_xAl_yF_zO$ thin films

Zinc oxide (ZnO) thin films were fabricated using an aqueous solution (40 ml in volume) of 0.1 M zinc acetate, with and without aluminum (Al) + fluorine (F) doping. The films were deposited on glass substrates with dimensions of $70 \times 20 \times 1.5 \text{ mm}^3$, which were thoroughly cleaned using organic solvents. The deposition process was carried out at a substrate temperature of 325°C . The precursor solution was sprayed intermittently onto pre-heated substrates using a fragrance vaporizer. This intermittent spray procedure involved alternating

between spraying and a 5 s pause to maintain the desired substrate temperature throughout the deposition process. During the spraying process, the aqueous solution of pure zinc acetate and [Al + F]-doped zinc acetate underwent pyrolytic decomposition upon contact with the hot substrates, leading to the formation of thin films.

2.2. Structural, morphological and optical studies

In the characterization of aluminum and fluorine ([Al + F]) co-doped ZnO thin films, various analytical techniques are employed to assess their structural, optical, and electrical properties. These techniques include X-ray diffraction (XRD), Fourier transform infrared spectroscopy (FTIR), electrical measurements, optical transmission studies, photoluminescence (PL) spectroscopy, and scanning electron microscopy (SEM) with energy dispersive X-ray spectroscopy (EDX). The instruments used for these analyses are X-ray diffractometer (PANalytical PW 340/60 X'Pert PRO), FTIR spectrometer (Nicolet iS20), four-point linear probe (SES Instruments DFP-RM-200), ultraviolet-visible-near-infrared (UV-Vis-NIR) double beam spectrophotometer (PerkinElmer LAMBDA 35), photoluminescence spectrometer (FLS1000), scanning electron microscope with EDX (JEOL JSM-6701F). These instruments facilitate a comprehensive analysis of the thin films, providing insights into their crystallographic structure, chemical composition, surface morphology, and functional properties.

TABLE I

Structural parameters of AFZnO films: lattice constants, crystallite size (D), dislocation density (δ), strain (ϵ), volume of the unit cell (V), and specific surface area (S).

[Al + F] doping level in the precursor solution [at.%]	Lattice parameter		D [nm]	δ ($\times 10^{15}$) [cm ⁻³]	ϵ ($\times 10^{-3}$)	V ($\times 10^{-30}$) [m]	S ($\times 10^3$) [m ² /g]
	a	c					
	[m]						
0+0	3.2555	5.2092	71.20	0.1972	1.58	47.810	14.823
3 + 5	3.2544	5.2047	63.09	0.2512	1.79	47.737	16.964
3 + 10	3.2410	5.1856	54.17	0.3408	2.09	47.170	19.759
3 + 15	3.2361	5.1787	52.64	0.3609	2.15	46.965	20.333
3 + 20	3.2342	5.1727	41.36	0.5846	2.72	46.856	25.879

For instance, XRD analysis can confirm the crystalline structure of the ZnO thin films, ensuring the incorporation of dopants without altering the wurtzite structure. FTIR spectroscopy can identify functional groups and bonding structures, providing insights into the chemical composition and confirming the presence of specific dopants. Electrical measurements assess the conductivity of the films, which is crucial for applications in electronic devices. Optical transmission studies evaluate the transparency of the films in the visible range, which is advantageous for applications requiring transparent electrodes. PL spectroscopy provides information on the electronic and defect states within the films, which is essential for understanding their optical properties and potential applications in optoelectronic devices. SEM images reveal the surface morphology and grain structure of the films, while EDX analysis confirms the elemental composition, verifying the successful incorporation of aluminum and fluorine dopants.

These characterization techniques collectively provide a comprehensive understanding of the structural, optical, and electrical properties of [Al + F]:ZnO thin films, facilitating their optimization for various technological applications.

3. Results and discussion

3.1. Surface morphology and elemental analysis

The scanning electron microscope (SEM) images of pristine and AlFZnO films deposited with varying [Al + F]/Zn ratios are presented in Fig. 1a–e. These images reveal very smooth surfaces, free of pinholes, with uniformly distributed and well-defined spherical grains. As the [Al + F]/Zn ratio increases, as observed in Fig. 1c–e, the surface becomes more compact, and the grain size decreases. The SEM image of the ZnO film shows crystallite sizes that are in good agreement with those obtained from X-ray diffraction (XRD) results.

The energy dispersive spectroscopy (EDS) spectrum (see Fig. 1f) confirms the presence of the expected elements — Zn, Al, F, and O — in the deposited film. The accompanying table provides the atomic and weight proportions of these elements.

These morphological changes can significantly influence the optical and electrical properties of the films, making them suitable for various applications in optoelectronic devices.

3.2. Crystalline structure and crystallite size

Figure 2 shows the X-ray diffractogram (XRD) of [Al + F] co-doped ZnO thin films synthesized using the simplified spray technique. Figure 2 shows the peak (002), which indicates the preferential crystallographic orientation of the films. It consistently shows the highest intensity across all doping levels. However, an increase in fluorine doping leads to a noticeable reduction in the peak intensity, as reported by Ilıcan et al. [18]. The ZnO crystal’s polycrystalline, hexagonal wurtzite structure is confirmed by the spectra and the peak position corresponding to the data card of the Joint Committee on Powder Diffraction Standards (JCPDS 36-1451). From the XRD patterns, the other characteristic peaks, such as Zn(OH)₂, Zn, Al, Al₂O₃, and zinc fluorine compounds, appeared even at the highest simultaneous doping. It has been discovered that the (002) plane’s crystallographic preference orientation evolves on the substrate’s surface perpendicular to the c -axis. Preferential orientation of this kind is typically observed in ZnO films co-doped with fluorine and aluminum. Subsequently, ZnO films doped with [Al + F] are referred to as AlFZnO films. The presence and characteristics of the (101) peak provide valuable insights into the films’ structural properties. The (101) peak, along with the (002) peak, is indicative of the hexagonal wurtzite structure of ZnO. The relative intensities and positions of these peaks can reveal information about the crystallographic orientation, crystallite size, and

the effects of doping on the crystal lattice. The lattice parameters “ a ” and “ c ” of the hexagonal wurtzite structure have been calculated by using [19]

$$\frac{1}{d^2} = \frac{4}{3} \frac{(h^2 + hk + k^2)}{a^2} + \frac{l^2}{c^2}. \quad (1)$$

From Table I, the lattice constant c is found to decrease from 5.2092 for ZnO film to 5.1727 for AlFZnO film with 3 + 20 at.% of [Al + F] doping. The decrease in the c value probably occurs due to the substitutional incorporation of Al^{3+} ions into Zn^{2+} sites and also because the ionic radius of Al^{3+} (0.53 Å) ions is observed to be substantially less than that of Zn^{2+} (0.72 Å) ions. Furthermore, the oxygen atom is replaced by a fluorine atom, and the ionic radii of F^- (1.33 Å) are nearly equal to the ionic radius of O^{2-} (1.32 Å) [20]. This decreases the c value, which must be the consequence of the change in the interplanar distance (d) values as $d = c/2$ for the hexagonal wurtzite structure. The crystallographic (002) peak shifts towards the higher angle (θ) with increasing [Al + F] concentration in AlFZnO films, resulting in a decrease in lattice parameter in the direction of the c axis. Salim et al. [21] observed the same trend in the Al-alone ZnO film. In [Al + F] co-doped ZnO thin films with a hexagonal wurtzite structure, the volume of the hexagonal unit cell (V) is estimated with the formula

$$V = \frac{\sqrt{3}}{2} a^2 c. \quad (2)$$

Accurate determination of these lattice parameters is essential for understanding the effects of co-doping on the crystal structure and properties of ZnO thin films.

The crystalline size of the deposited films is calculated using Debye–Scherrer’s formula [22]

$$D = \frac{K\lambda}{\beta \cos(\theta)}, \quad (3)$$

where D is the crystallite size of the ZnO film [nm], λ is the wavelength of the X-ray used, β is the full width at half maximum, and θ is the angle of diffraction. The following equation is used to calculate the dislocation density of the deposited films [23]

$$\delta = \frac{1}{D^2}. \quad (4)$$

It is also important to mention the amount of dislocations, such as lattice imperfections, present in the thin films. The micro-strain of the films is calculated using the formula given by [24]

$$\epsilon = \frac{\beta \cos(\theta)}{4}. \quad (5)$$

The crystallite size for the pristine ZnO thin film is calculated as 73 nm. In the [Al + F]-doped zinc oxide films, the grain size reduces gradually (37 nm) with an increase in [Al + F] doping level in the precursor solution. Hence, the doping

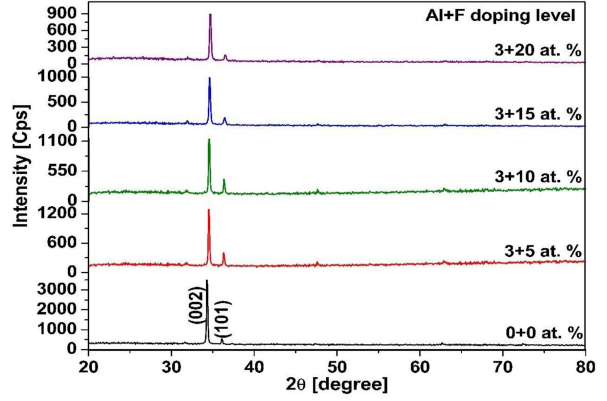


Fig. 2. XRD patterns of [Al + F]-doped ZnO films.

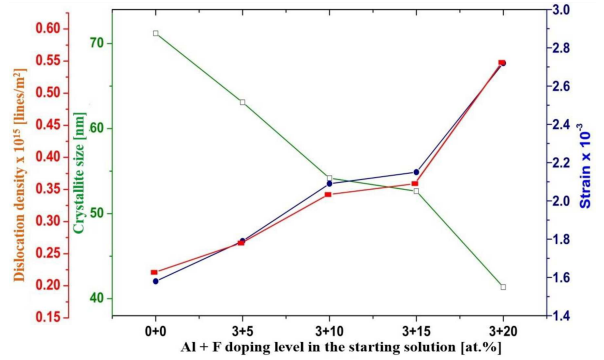


Fig. 3. Grain size, strain, and dislocation density evolutions of ZnO and AlFZnO samples.

with [Al + F] ions simultaneously diminishes the crystalline quality of the pristine ZnO crystal. Consequently, the dislocation density of the film increases, indicating a decrease in the degree of crystallinity of the film. Furthermore, as seen in Fig. 3, the predicted dislocation density increases as the fluorine concentrations increase, most likely due to fluorine occupying interstitial sites and grain boundaries. It is observed that the lattice parameters (a and c) and unit cell volume decrease as the amount of fluorine content increases. The specific surface area (SSA) is a material characteristic that is used to calculate the total surface area of the crystals per unit of mass. The specific surface area helps evaluating the optimized adsorption and reactions of foreign atoms, such as catalysts, on the surface of the deposited films. The SSA value is estimated by the Sauter equation [25]

$$S = \frac{6 \times 10^3}{D\rho}, \quad (6)$$

where ρ is the density of the bulk form of zinc oxide crystal (5.606 g/cm³), and D is the crystal size. The SSA of films was enhanced with the increase in [Al + F] simultaneous doping level in the ZnO matrix. The calculated structural parameter values are given in Table I.

3.3. Functional group analysis

Attenuated total reflectance (ATR) is a sampling method that is used to obtain the structural and compositional information from a sample. It is also useful for monitoring the chemical reactions. ATR is one of the most commonly utilized sampling technologies in FTIR spectroscopy. It is a good approach for analyzing thin film samples. ATR-FTIR spectra of ZnO thin films are deposited with different [Al + F] dopants using zinc acetate, as illustrated in Fig. 4. Generally, the bands at 411–427 cm^{-1} and 761 cm^{-1} represent the stretching vibration of the Zn–O bond in the hexagonal ZnO crystal. The band is located at 887–894 cm^{-1} with a Zn–O–H (zinc hydroxyl group) vibration.

Figure 4 depicts the FTIR spectra of AlFZnO thin film acquired in the 400–4000 cm^{-1} region using the KBr pellet method. Figure 4 shows that a significant absorption peak at 423 cm^{-1} corresponds to the stretching vibration of AlFZnO (10%). Furthermore, we discovered that the significant absorption peaks at 661, 770, and 850 cm^{-1} are due to the presence of carbonate moieties, which are commonly detected when FTIR measurements are performed in an air atmosphere for AlFZnO (20%). Three significant absorption peaks were detected in AlFZnO (30%) nanoparticles at 689, 762, and 875 cm^{-1} . The signal at 754 cm^{-1} reveals the presence of AlFZnO's (30%) stretching vibration.

The characteristic absorption band for the Al–O stretching mode is seen between 580–620 cm^{-1} . In the current study, there are no other peaks associated with the Al–O mode of vibration. However, for AlFZnO (40%) nanoparticles, the absorption peaks at 683, 754, and 871 cm^{-1} are very prominent. Stretching bands in the 500–900 cm^{-1} range are related to vibrations of metal–oxygen, aluminum–oxygen, and metal–oxygen–aluminum [26–28].

The doped samples exhibit two peaks at about 500 and 900 cm^{-1} for all nanomaterials, indicating metal aluminate production. Figure 4 illustrates the FTIR spectra of ZnO thin film composites with substantial attenuation of the peak, indicating that each nanoparticle is coated with aluminum and fluorine [29]. These large alterations are due to chemical interactions between AlFZnO thin films. This leads to better conjugation or chain length.

3.4. Photocatalytic studies

Nanomaterials are highly reactive due to their enormous surface area. ZnO has the highest photocatalytic efficiency of any inorganic photocatalytic material, and it responds strongly to UV light, which dramatically activates its contact with bacteria. ZnO thin films exhibit a phototoxic action that generates reactive oxygen species, which are vital

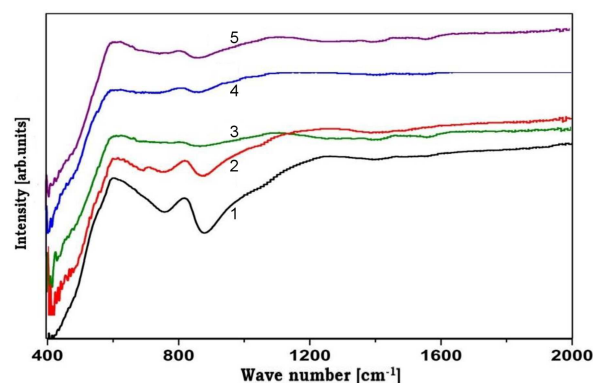


Fig. 4. FTIR spectra of different [Al + F]-doped ZnO films: line 1 — 0+0 at.%, line 2 — 3 + 5 at.%, line 3 — 3 + 10 at.%, line 4 — (d) 3 + 15 at.%, line 5 — 3 + 20 at.%.

for biological applications. Adding selective dopants to ZnO thin film improves photocatalytic activity and Z-scheme mechanism, leading to an increase in visible light and antimicrobial action. It has been demonstrated that nanoparticles can be synthesized using a variety of physical, chemical, and biological processes [30].

Aluminum and fluorine were chosen as dopants for ZnO semiconductors due to their availability, low cost, and compatibility. According to several publications, adding Al and F to the zinc oxide crystal lattice improves conductivity by n-type doping. The crystallographic location of the aluminum dopant in the ZnO lattice has been found to alter the electronic characteristics of the doped oxide. Al and F ions can occupy empty tetrahedral positions and replace Zn^{2+} ions in tetrahedral geometry, providing a free electron and improving conductivity. Similarly, Al and F ions can occupy an interstitial octahedral coordinated position. The presence of Al and F ions in the octahedral location reduces conductivity and further optimizes the electronic characteristics of the ZnO host material, arranging the Al and F dopants in a substitutional, tetrahedral location. The use of post-transition metals as dopants causes flaws that contribute to improved functionality. To study photocatalytic degradation under UV–visible light, the synthesized and characterized Al- and F-doped ZnO thin films with increasing amounts of (10–40%) aluminum and fluorine relative to ZnO are shown in Fig. 5. Although several authors have reported on Al and F-doped ZnO thin films, it is difficult to compare their photocatalytic performances directly due to non-standardized variables such as reaction conditions, light source, and reactor configuration [31].

Figure 5 displays the variation of the absorption spectra at different decolorization periods using AlFZnO thin films, revealing that the peak of the absorption spectra decreases as the decolorization doping percentage grows from 10 to 40 at.%. As is

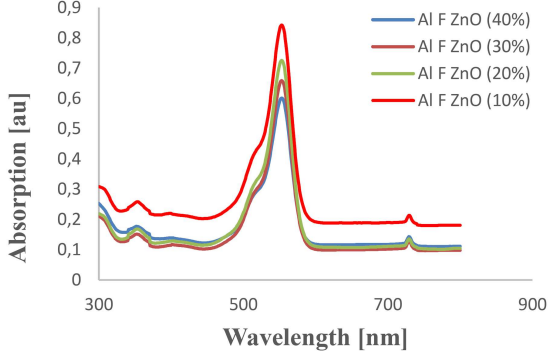


Fig. 5. Photocatalytic analysis of AlFZnO nanoparticles for various doping percentages.

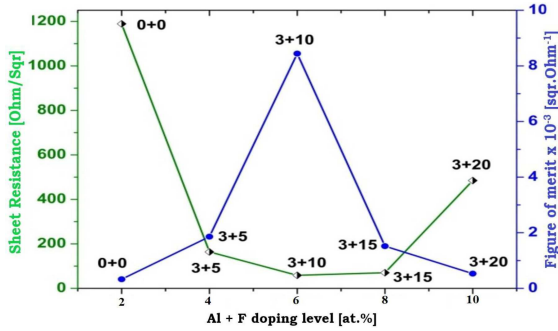


Fig. 6. Sheet resistance and figure of merit graph of [Al + F]-doped ZnO films.

widely known, AlFZnO has remarkable photocatalytic activity in the removal of dye-contaminated wastewater and harmful organic substances [32–33]. However, one of the fundamental disadvantages of ZnO thin films is their rapid electron–hole pair recombination. In this scenario, the presence of Al and F allows for the effective separation of the electron–hole couple [34–35].

Combining zinc (Zn) with aluminum (Al) and fluorine (F) to form zinc oxide (ZnO) creates more reactive sites on the surface, which helps in adsorbing more molecules. As a result, adsorption centers form, allowing dye molecules to be adsorbed more effectively. The addition of aluminum and fluorine can increase the rate of transit of photoinduced electrons from the valence band of ZnO to the conducting band of ZnO, which aids in the separation of electrons and holes, thereby improving the photocatalytic activity of ZnO under visible light [36–37].

Photoinduced electrons are adsorbed on the structural defects of aluminum and fluorine, and electrons from ZnO can be transferred to aluminum and then fluorine, extending the length of electron–hole pair recombination [38]. Hydroxyl ions and H₂O molecules can combine with holes on the ZnO surface to produce hydroxyl radicals (OH), which have a high oxidation potential. Surface-bound (OH) radicals can oxidize substrates [39]. Dissolved

oxygen can combine with photoinduced electrons to generate superoxide radical anions (O²⁻) on the ZnO surface [40], which then react with H₂O or Hydroxyl ions to form OH radicals that participate in the photocatalytic activity [41]. Surface oxidation–reduction processes, charge separation and migration, and photoexcitation are frequently included in photocatalytic reactions [42].

3.5. Electrical study

The type of conductivity of the films is measured using the hot probe technique. *N*-type conductivity is found to be exhibited by all the deposited thin films. The sheet resistance (R_{sh}) of the pristine and AFZnO films is shown in Fig. 6. From this investigation, it is concluded that the sheet resistance of the pristine film has a higher R_{sh} value of 1.189 K Ω . It confirms that the pristine ZnO lattice has a good stoichiometric nature. However, [Al + F]-doped films (3 + 10 at.%) have a minimum R_{sh} value of 58.75 K Ω . This decreases the R_{sh} value, which can be confirmed by replacing Zn²⁺ atoms with Al³⁺ atoms and substituting F⁻ in O²⁻ site. As a result, [Al³⁺ + F⁻] ions give more electrons to the conduction band, which results in an increase in the electron density of the conduction band. Furthermore, the doping level is increased to 3 + 20 at.% and the R_{sh} value increases as follows: (i) decreasing the trend of oxygen vacancy, (ii) decreasing the level of Zn interstitial position. This can be attributed to the production of crystal disorders in the lattice. However, this disorder mechanism increases the phonon scattering, which in turn increases the R_{sh} value. To the best of the author’s knowledge, this represents the lowest sheet resistance value reached for sprayed AlFZnO films.

3.6. Optical study

Figure 7 shows the optical transmittance spectra of [Al + F]-doped ZnO films. The spectra have been recorded between 300 and 1100 nm. The absorption coefficient α is estimated from Lambert’s law using the transmittance spectra

$$\alpha = \frac{1}{t} \ln \left(\frac{1}{T} \right), \quad (7)$$

where α is the absorption coefficient of the material, t is the thickness of the film, and T is the transmittance of the film. The deposited films have an average optical transmittance in the visible region of about 90%. The high visible transmittance of the films is due to the intrinsic direct wide band gap property of the ZnO crystal. While increasing the [Al + F] doping level (Al = 3 at.% and F = 5, 10, 15, and 20 at.%), the absorption edge shifts towards the lower wavelength (blue shift) of the region. This is due to the number of [Al + F] atoms that are

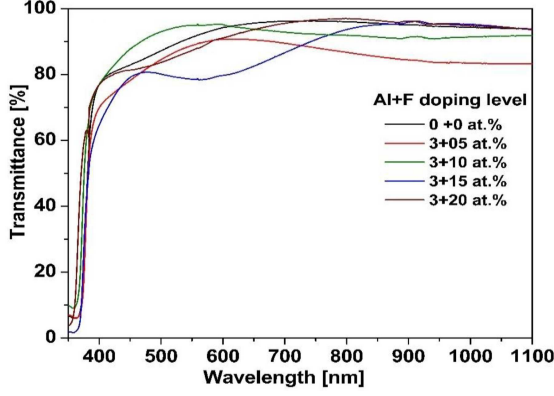


Fig. 7. Optical transmittance spectra of [Al + F]-doped ZnO films.

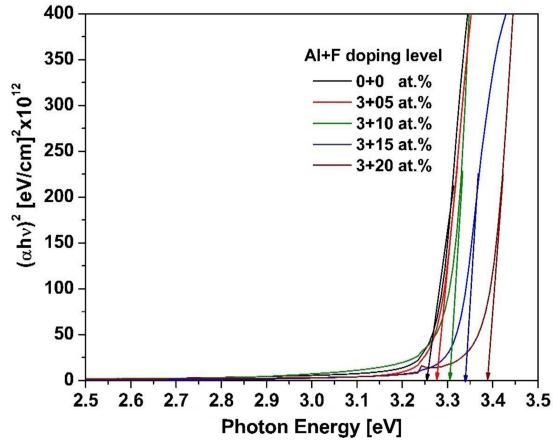


Fig. 8. Tauc's plot of [Al + F]-doped ZnO films.

strongly incorporated into the ZnO crystal lattice and can be attributed to the slight loss in crystallinity, lifting of the Fermi level in the conduction band, and the Moss–Burstein effect [43]. The optical band gap is estimated using the given formula

$$\alpha h\nu = A(h\nu - E_g)^{1/2}, \quad (8)$$

where $h\nu$ is the photon energy of the incident light, A is the constant, and E_g is the energy gap of the film. The band gap of the deposited films is calculated using Tauc's plot (Fig. 8). The extrapolation of the linear portion of the $(\alpha h\nu)^2$ vs $h\nu$ plots shows the energy band gap of the pristine and AlFZnO film. The band gap value increases from 3.25 to 3.38 eV and is consistent with the recent literature [44]. The films must have a low resistance and a high optical transparency in order to be used as transparent electrodes in solar cells. The figure of merit (FOM) is one of the methods for analyzing the above-mentioned applications. FOM, as defined by Haacke [45], is one of the most essential indicators for evaluating the efficacy of various processes. The FOM values are calculated using the formula

$$\text{FOM} = T^{10}/R_{sh}, \quad (9)$$

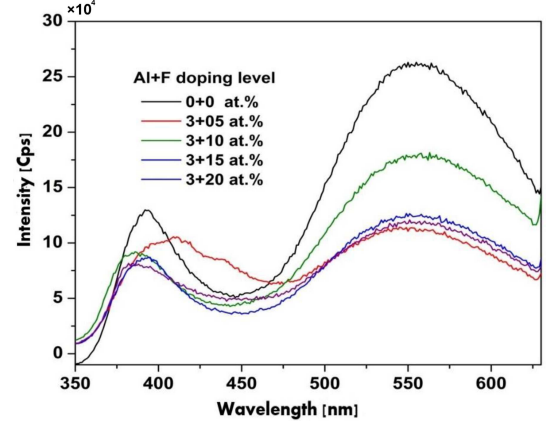


Fig. 9. Photoluminescence spectra of [Al + F]-doped ZnO films.

where T is the average optical transmittance (at 550 nm) and R_{sh} is the sheet resistance of films (see Fig. 6). The highest FOM value ($8.44 \times 10^{-3} \Omega/\square$) is obtained in the film doped with 3 + 10 at. 1% [Al + F]. Comparing with the literature [46], the result is found to be higher than others.

3.7. Photoluminescence study

The photoluminescence (PL) spectra of pristine and [Al + F]-doped ZnO thin films are shown in Fig. 9. There are two luminescence bands in the PL spectra, namely sharp ultraviolet (UV) emission (band gap excitation) from crystalline ZnO, and recombination of free excitons around 375 nm. Generally, this visible emission is referred to as deep-level emission, which is related to the oxygen vacancy, interstitial zinc (Zn_i), or interstitial oxygen (O_i). The bulk oxygen vacancies produce more recombination centers. In addition, the broad green emission peak is visible at 554 nm. This emission is ascribed to singly ionized oxygen vacancies (V_O). The peak intensity further decreases for Al and F co-doped samples. This can be attributed to diminishing the oxygen vacancies. Therefore, the doubly doped sample enhances the charge separation rate, resulting in a lower recombination rate of electron-hole pairs, as expected.

4. Conclusions

This work aims to fabricate pristine and Al and F co-doped ZnO thin films using a cost-effective spray pyrolysis technique. Aluminum and fluorine doping concentrations in the precursor solutions are in the range of 0, 3 + 5, 3 + 10, 3 + 15, and 3 + 20 at.%. XRD spectra indicate that the films

are polycrystalline, with the peak (002) showing maximum intensity across all doping levels. Structural parameters, including crystallite size, unit cell volume, dislocation density, and strain, were calculated. The films' optical energy gap values range from 3.25 to 3.38 eV. The lowest electrical sheet resistance observed is $58.75 \Omega/\square$, with a high figure of merit at $8.441 \times 10^{-3} \square^{-1}$. These findings suggest that this simplified spray pyrolysis technique is a low-cost and effective method for producing transparent electrodes in optoelectronic applications.

References

- [1] P. Velusamy, R. Xing, R. Ramesh Babu, E. Elangovan, J. Viegas, S. Liu, M. Sridharan, *Sens. Actuators B Chem.* **297**, 126718 (2019).
- [2] J. Shanthi, S. Aishwarya, R. Swathi, *Chem. Data Collect.* **29**, 100494 (2020).
- [3] C.-H. Ho, C.-H. Chan, L.-C. Tien, Y.-S. Huang, *J. Phys. Chem. C* **115**, 25088 (2011).
- [4] S. Sambasivam, P.S. Maram, C.V.V. Muralee Gopi, I.M. Obaidat, *Optik* **202**, 163596 (2020).
- [5] T. Amakali, L.S. Daniel, V. Uahengo, N.Y. Dzade, N.H. de Leeuw, *Crystals* **10**, 132 (2020).
- [6] A.K. Ambedkar, M. Singh, V. Kumar, V. Kumar, B.P. Singh, A. Kumar, Y.K. Gautam, *Surf. Interfaces* **19**, 100504 (2020).
- [7] L.H. Kathwate, G. Umadevi, P.M. Kulal, P. Nagaraju, D.P. Duba, A.K. Nanjundan, V.D. Mote, *Sens. Actuators A Phys.* **313**, 112193 (2020).
- [8] W. Li, H. Yin, H. Mo, L. Lai, S. Fu, L. Li, L. Ye, Y. Xiong, H. Li, *Thin Solid Films* **713**, 138350 (2020).
- [9] V. Ganesh, I.S. Yahia, S. AlFaify, M. Shkir, *J. Phys. Chem. Solids* **100**, 115 (2017).
- [10] P. Thilakan, D.M. Radheep, K. Saravanakumar, G. Sasikala, *Semicond. Sci. Technol.* **24**, 085020 (2009).
- [11] E. Gunasekaran, M. Ezhilan, G.K. Mani, P. Shankar, A.J. Kulandaisamy, J.B. Balaguru Rayappan, K. Jayanth Babu, *Semicond. Sci. Technol.* **33**, 095005 (2018).
- [12] Guoxi Zheng, Jianmin Song, Jie Zhang, Junjie Li, Bing Han, Xudong Meng, Fu Yang, Ying Zhao, Yanfeng Wang, *Mater. Sci. Semicond. Process.* **112**, 105016 (2020).
- [13] V.K. Kaushik, C. Mukherjee, P.K. Sen, *J. Mater. Sci. Mater. Electron.* **29**, 15156 (2018).
- [14] S. Edinger, N. Bansal, M. Bauch, R.A. Wibowo, R. Hamid, G. Trimmel, T. Dimopoulos, *J. Mater. Sci.* **52**, 9410 (2017).
- [15] K. Deva Arun Kumar, S. Valanarasu, V. Ganesh, M. Shkir, A. Kathalingam, S. AlFaify, *J. Electron. Mater.* **47**, 1335 (2018).
- [16] Woo Jun Seol, Gopinathan Anoop, Hyeonhun Park, Cheol Woong Shin, Jun Young Lee, Tae Yeon Kim, Wan Sik Kim, Hyunjin Joh, Shibnath Samanta, Ji Young Jo, *J. Alloys Compd.* **853**(5), 157369 (2021).
- [17] P. Thilakan, D. Mohan Radheep, K. Saravanakumar, G. Sasikala, *Semicond. Sci. Technol.* **24**, 085020 (2009).
- [18] S. Ilican, Y. Caglar, M. Caglar, F. Yakuphanoglu, *Appl. Surf. Sci.* **255**, 2353 (2008).
- [19] K. Saravanakumar, K. Ravichandran, *J. Mater. Sci. Mater. Electron.* **23**, 1462 (2012).
- [20] K. Saravanakumar, B. Sakthivel, K. Ravichandran, *Mater. Lett.* **65**, 2278 (2011).
- [21] K. Salim, M. Medles, A. Nakrela, R. Miloua, A. Bouzidi, R. Desfeux, *Optik* **210**, 164504 (2020).
- [22] K. Saravanakumar, K. Ravichandran, R. Chandramohan, S. Gobal Krishnan, M. Chavali, *Superlatt. Microstruct.* **52**, 528 (2012).
- [23] E. Indrajith Naik, H.S. Bhojya Naik, R. Viswanath, I.K. Suresh Gowda, M.C. Prabhakara, *SN Appl. Sci.* **2**, 863 (2020).
- [24] M. Jothibas, C. Manoharan, S.J. Jeyakumar, P. Praveen, I.K. Punithavathy, J.P. Richard, *Sol. Ener.* **159**, 434 (2018).
- [25] P.U. Aparna, N.K. Divya, P.P. Pradyumnann, *MSCE* **4**, 79 (2016).
- [26] Z.X. Deng, C. Wang, X.M. Sun, Y.-D. Li, *Inorg. Chem.* **41**, 869 (2002).
- [27] K. Nakamoto, *Infrared and Raman Spectra of Inorganic and Coordination Compounds: Part A: Theory and Applications in Inorganic Chemistry*, 4th ed., Chemical Industry Press, Beijing, 1991.
- [28] L.K.C. de Souza, J.R. Zamian, G.N. da Rocha Filho, L.E.B. Soledade, I.M.G. dos Santos, A.G. Souza, T. Scheller, R.S. Angelica, C.E.F. da Costa, *Dyes Pigments.* **81**, 187 (2009).

- [29] A. Batool, F. Kanwal, M. Imran, T. Jamil, S. Anwar Siddiqi, *J. Synth. Mate.* **161**, 2753 (2012).
- [30] A. Chauhan, R. Verma, S. Kumari, A. Sharma, P. Shandilya, X. Li, K. Mujasam Bato, A. Imran, S. Kulshrestha, R. Kumar, *Sci. Rep.* **10**, 7881 (2020).
- [31] A. Piras, C. Olla, G. Reekmans et al., *Int. J. Mol. Sci.* **23**, 15459 (2022).
- [32] A.L. Desa, N.H.H. Hairom, D.A.B. Sidik, N. Misdan, N. Yusof, M.K. Ahmad, A.W. Mohammad, *J. Environ. Chem. Eng.* **7**, 103143 (2019).
- [33] D. Xu, J. Li, J. Liu, X. Qu, H. Ma, *Environ. Prot.* **163**, 27 (2022).
- [34] G. Meenakshi, A. Sivasamy, *Colloids Surf. A Physicochem. Eng. Asp.* **645**, 128920 (2022).
- [35] C.M. Gomez, G.D. Angel, E. Ramos-Ramírez, I. Rangel-Vázquez, F. González, A. Arrieta, A. Vázquez-Zavala, A. Bonilla-Sanchez, M. Sanchez Cantú, *J. Chem. Technol. Biotechnol.* **91**, 2211 (2016).
- [36] P.A.L. Anawe, O. Fayomi, A. Popoola, *Results Phys.* **7**, 777 (2017).
- [37] A.C. Aragones, A. Palacios-Padros, F. Caballero-Briones, F. Sanz, *Electrochim. Acta.* **109**, 117 (2013).
- [38] H. Deng, Y. Wang, X. Zhang, X. Kou, B. Chen, C. Zhu, *Chem. Eng. J.* **372**, 99 (2019).
- [39] M. El-Kemary, H. El-Shamy, I. El-Mehasseb, *J. Lumin.* **130**, 2327 (2010).
- [40] N. Li, J. Zhang, Y. Tian, J. Zhao, J. Zhang, W. Zuo, *Chem. Eng. J.* **308**, 377 (2017).
- [41] Y. Nosaka, S. Komori, K. Yawata, T. Hirakawa, A.Y. Nosaka, *Phys. Chem. Chem. Phys.* **5**, 4731 (2003).
- [42] W. Liu, T. He, Y. Wang, G. Ning, Z. Xu, X. Chen, X. Hu, Y. Wu, Y. Zhao, *Sci. Rep.* **10**, 11903 (2020).
- [43] E. Burstein, *Phy. Rev.* **93**, 632 (1954).
- [44] S. Atiq, M. Tamoor Ansar, A. Hassan, S. Kumail Abbas, T. Iqbal, M. Aslam, M. Javaid Iqbal, A. Mahmood, *Superlatt. Microstruct.* **144**, 106576 (2020).
- [45] G. Haacke, *J. Appl. Phys.* **47**, 4086 (1976).
- [46] S.S. Shinde, P.S. Shinde, S.M. Pawar, A. Moholkar, C.H. Bhosale, K.Y. Rajpure, *Solid State Sci.* **10**, 1209 (2008).